AGU PUBLICATIONS

Geochemistry, Geophysics, Geosystems

RESEARCH ARTICLE
10.1002/2016GC006550

Rapid variations in fluid chemistry constrain hydrothermal phase separation at the Main Endeavour Field

Brooke Love[1], Marvin Lilley[2], David Butterfield[3], Eric Olson[2], and Benjamin Larson[3]

[1]Huxley College of the Environment, Western Washington University, Bellingham, Washington, USA, [2]School of Oceanography, University of Washington, Seattle, Washington, USA, [3]University of Washington, JISAO and NOAA, Pacific Marine Environmental Lab, Seattle, Washington, USA

Key Points:
- High frequency sampling captured an excursion in fluid chemistry, clarifying constraints on phase separation and mixing processes.
- The most likely explanations include brine condensation at depth followed by near-critical phase separation and mixing.
- Multidimensional data sets including gasses help interpret variability in records of temperature and salinity in hydrothermal systems.

Supporting Information:
- Supporting Information S1

Correspondence to:
B. Love,
Brooke.Love@wwu.edu

Citation:
Love, B., M. Lilley, D. Butterfield, E. Olson, and B. Larson (2017), Rapid variations in fluid chemistry constrain hydrothermal phase separation at the Main Endeavour Field, *Geochem. Geophys. Geosyst.*, *18*, 531–543, doi:10.1002/2016GC006550.

Received 25 JUL 2016
Accepted 9 DEC 2016
Accepted article online 29 DEC 2016
Published online 7 FEB 2017

Abstract Previous work at the Main Endeavour Field (MEF) has shown that chloride concentration in high-temperature vent fluids has not exceeded 510 mmol/kg (94% of seawater), which is consistent with brine condensation and loss at depth, followed by upward flow of a vapor phase toward the seafloor. Magmatic and seismic events have been shown to affect fluid temperature and composition and these effects help narrow the possibilities for sub-surface processes. However, chloride-temperature data alone are insufficient to determine details of phase separation in the upflow zone. Here we use variation in chloride and gas content in a set of fluid samples collected over several days from one sulfide chimney structure in the MEF to constrain processes of mixing and phase separation. The combination of gas (primarily magmatic CO_2 and seawater-derived Ar) and chloride data, indicate that neither variation in the amount of brine lost, nor mixing of the vapor phase produced at depth with variable quantities of (i) brine or (ii) altered gas rich seawater that has not undergone phase separation, can explain the co-variation of gas and chloride content. The gas-chloride data require additional phase separation of the ascending vapor-like fluid. Mixing and gas partitioning calculations show that near-critical temperature and pressure conditions can produce the fluid compositions observed at Sully vent as a vapor-liquid conjugate pair or as vapor-liquid pair with some remixing, and that the gas partition coefficients implied agree with theoretically predicted values.

Plain Language Summary When the chemistry of fluids from deep sea hot springs changes over a short time span, it allows us to narrow down the conditions and processes that created those fluids. This gives us a better idea what is happening under the seafloor where the water is interacting with hot rocks and minerals, boiling, and taking on the character it will have when it emerges at the seafloor. Gasses like argon can be especially helpful here. We found that the fluids we sampled must have been formed by multiple boiling (phase separation) events, and that one of these would have to be close to the critical point of these fluids.

1. Introduction

Phase separation exerts major controls on fluid chemistry in many hydrothermal systems, which in turn affects fluid rock equilibria, fluxes of volatiles and metals, mineral deposition, and the resources and habitat available to biological communities. Variability in phase separation can therefore have far reaching implications in these systems. Phase separation may occur deep in the crust, or near the seafloor, and may be followed by segregation of the fluids that are formed, re-equilibration with mineral assemblages, or mixing with seawater or other hydrothermal fluids. The exact history of a fluid is therefore difficult to ascertain.

The Main Endeavour Field (MEF), located at 47°57N and 129°05W, on the Juan de Fuca Ridge, is notable for venting fluids of low and relatively stable salinity (quantified by chloride concentration) between when they were first observed in 1984 [*Butterfield et al*., 1994] and through the 1990s [*Lilley et al*., 2003; *Seewald et al*., 2003; *Seyfried et al*., 2003]. Gradients in chloride were present across the MEF, and many other elements were well correlated with chloride in a manner consistent with phase separation as a driving process. These patterns were relatively stable until June of 1999, when an earthquake swarm was detected and later interpreted as a magmatic event [*Johnson et al*., 2000; *Bohnenstiehl et al*., 2004]. Fluid chemistry data collected in the aftermath of this event helped verify its magmatic origins and described significant geochemical changes [*Lilley et al*., 2003; *Seewald et al*., 2003; *Seyfried et al*., 2003].

Evidence supporting a magmatic event includes large transient increases in magmatically derived He and CO_2, and decreases in Cl to as low as 32 mmol/kg compared with values of about 150 mmol/kg at that location prior to the event [*Lilley et al*., 2003]. New constraints on water rock reactions and equilibria as well as phase separation were also derived from data collected in the period following the disturbance in 1999. In particular, *Seyfried et al*. [2003] suggested that patterns in metal concentrations illustrated the interplay between the influence of temperature, pH, and chloride on metal solubility, as well as mixing of vapor and brine derived fluids. Solubility effects were shown to exert the most probable controls on H_2 and H_2S concentrations in the fluids [*Seewald et al*., 2003; *Seyfried et al*., 2003]. Fluids as MEF showed evidence of lower temperatures, higher water/rock ratios, and more oxidizing or lower temperature conditions in 2005 compared to 1999 and 2000 [*Foustoukos et al*., 2009].

Advances in instrumentation have allowed for increasingly fine scaled observations of temporal variability, which allow for increasingly detailed questions regarding the controls on fluid chemistry and flow. For instance, observations of relatively short term variability in fluid chemistry in this region include tidally driven oscillations in temperature and chloride at high temperature vents attributed to subsurface mixing of brines with near-critical fluids [*Larson et al*., 2009], as well as tidal variability in the temperature measured by the BARS sensor package deployed at the Grotto structure in the MEF [*Xu et al*., 2014]. Similar patterns are present in both high and low temperature flow in other systems, shedding light on the relative roles of tidal currents, tidal pressure and porosity structure on fluid characteristics [eg *Barreyre et al*., 2014; *Mittelstaedt et al*., 2016]. Modeling efforts can elucidate the effects of tidal loading on venting fluids [*Crone and Wilcock*, 2005], demonstrating the interplay between high resolution sampling and building an applied theoretical framework.

Many studies have covered the partitioning of seawater into vapor and liquid phases during phase separation, and how this partitioning varies with temperature and pressure [e.g., *Bischoff and Rosenbauer*, 1985; *Berndt et al*., 2001; *Driesner and Heinrich*, 2007a]. Briefly, when fluids enter the two-phase region, the composition of the two phases is determined by the temperature and pressure conditions. The relative quantity of each phase is controlled by the composition of the bulk fluid and can be determined through a simple mass balance. At a given pressure, higher temperatures will result in brine condensation, i.e., the production of a small quantity of highly saline liquid or brine, and a larger quantity of the vapor phase which has a composition similar to the original single-phase fluid. Brine condensation may result in storage of high-salinity brines in the crust [*Bischoff and Rosenbauer*, 1987; *Fontaine and Wilcock*, 2006]. In contrast, phase separation under conditions close to the critical point for a given fluid produces a vapor/liquid conjugate pair that are more similar to each other in composition and quantity and has been observed occurring close to the sea floor [*Von Damm et al*., 2003]. Finally, at lower temperatures, boiling can produce larger fractions of liquid and smaller fractions of low salinity, low density vapor.

It has been suggested that the primary mode of phase separation at MEF is brine condensation near the base of the convection cell [*Butterfield et al*., 1994; *Fontaine and Wilcock*, 2006]. This is supported by the largely stable record of chloride concentrations at this site with the exception of a volcanic disturbance in 1999 which appears to have caused significant changes, particularly in the southern MEF [*Butterfield et al*., 1994; *Lilley et al*., 2003; *Seyfried et al*., 2003; *Wilcock*, 2004; *Foustoukos et al*., 2009]. Both Seyfried et al. [2003] and Seewald et al. [2003] analyzed the fluid chemistry in the aftermath of the 1999 event and found observations could be explained by mixing of the vapor phase generated by brine condensation with seawater salinity hydrothermal fluid (hydrothermal source fluid). These findings were based upon several lines of reasoning including, metal concentrations, and the overall values and relative stability in estimated vapor partition coefficients.

A one-dimensional model for MEF predicted two zones of phase separation and two phase flow, both producing large fractions of vapor and small amounts of the liquid phase [*Seyfried et al*., 2003]. The reason that the fraction of brine remains small as the vapor phase rises in this and other models, is that as high salinity brines are segregated, the bulk salinity of the rising fluid is similar to that of the vapor which is created at each temperature and pressure, resulting in only modest amounts of brine to be produced thereafter, and very small changes in volatile concentrations in the vapor phase (Supporting information Figure S1).

Recent numerical modeling of the MEF also supported this model of deep brine condensation and added details of how permeability structure can influence spatial variability in fluid composition, providing support for this mechanism as a driver of gradients in chloride (and associated parameters) which existed between

northern and southern portions of the MEF, particularly prior to 1999 [*Singh et al.*, 2013]. Theoretical and numerical models are capturing the mechanisms in these systems with increasing sophistication, both in generalized models [*Coumou et al.*, 2009; *Han et al.*, 2013; *Weis et al.*, 2014] and models of specific hydrothermal areas [*Singh et al.*, 2013; *Gruen et al.*, 2014].

One numerical model, which simulated a system at a similar depth to the MEF, though with a shallower magma body, showed that brine condensation occurred in the base of the convection cell, and an unstable region of boiling developed near the seafloor [*Coumou et al.*, 2009]. A model of brine condensation followed by sub-critical vapor production was also indicated in earlier field data comparing Cl^- and CO_2 at the MEF [*Butterfield et al.*, 1994]. Here we present observations from the Sully structure in the MEF that appear to corroborate this model for two distinct zones of phase separation, while ruling out several other scenarios. They are not the only possibilities nor are there data to indicate that these conditions were persistent; however, they provide an example of how high resolution sampling can capture data important for understanding the underlying processes in a system.

2. Materials and Methods

Samples were collected with DSV Alvin and ROV Jason (Alvin 3570, 3577, 3580, 3582, Jason 279 and 280), into evacuated titanium gas tight bottles [*Edmond*, 1992] and on the PMEL Hydrothermal Fluid and Particle Sampler [*Butterfield et al.*, 2004]. One sample per dive was collected at this structure on most of these dives. However, on the two Jason dives, a higher frequency sampling campaign designed to detect tidal variability, captured a large fluid chemistry fluctuation.

Temperatures were acquired with either the DSV Alvin or ROV Jason high temperature probes. Several orifices on the Sully structure were sampled during this time series (Supporting information Table S2). Fluids were extracted from the sample bottles under vacuum and sealed into glass ampoules for later analysis of gas concentrations by gas chromatography where the components were separated using either Hayesep A or Hayesep Q porous polymer columns (18–24 ft × 1/8 inch) started at −50°C and ramped to 120°C. Sample injection was accomplished by expanding ampoule aliquots into a known-volume loop at measured temperature and pressure. Component detection and quantification took place on one of four detectors (TCD, FID, HID, or PDD). Standard error for CO_2, CH_4, and H_2 was ±3–5% of the measured value. H_2S concentrations were calculated by difference. Chloride and magnesium concentrations were determined by ion chromatography (Dionex DX500 with suppressed conductivity detection). The 1-sigma precision of the ion chromatography method based on long-term analysis of quality control samples is 0.5% for Cl and 1% for Mg. Dissolved silica was determined shipboard on acidified and diluted samples using the spectrophotometric silico-molybdate blue method [*Fanning and Pilson*, 1973], with precision of 0.5%. Sample aliquots from non-gas-tight samplers were acidified with ultra-pure HCl and analyzed for Fe and Mn by atomic absorption at PMEL with a precision of 4% [*Butterfield et al.*, 1994]. Gas-tight samples were not analyzed. All concentrations were corrected to a zero-magnesium hydrothermal endmember value to remove the influence of seawater entrained during sampling.

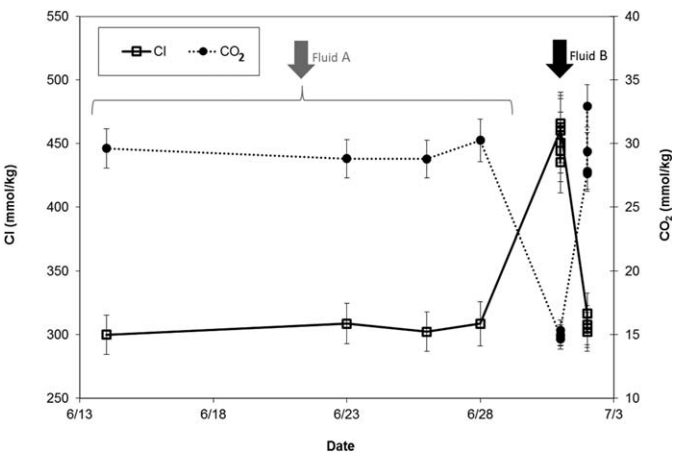

Figure 1. Endmember chloride and CO_2 concentrations, showing relatively stable fluid composition (fluid A) in samples pre- and post-dating 1 July. Samples collected on 1 July have a distinct composition with much higher chloride and lower gas content (Fluid B).

For phase separation calculations used to interpret these data, the salinities of the two phases produced when fluids encounter the two phase surface were calculated based on the P-T-X equations of Dreisner and Heinrich [2007a, 2007b]. A mass balance approach for

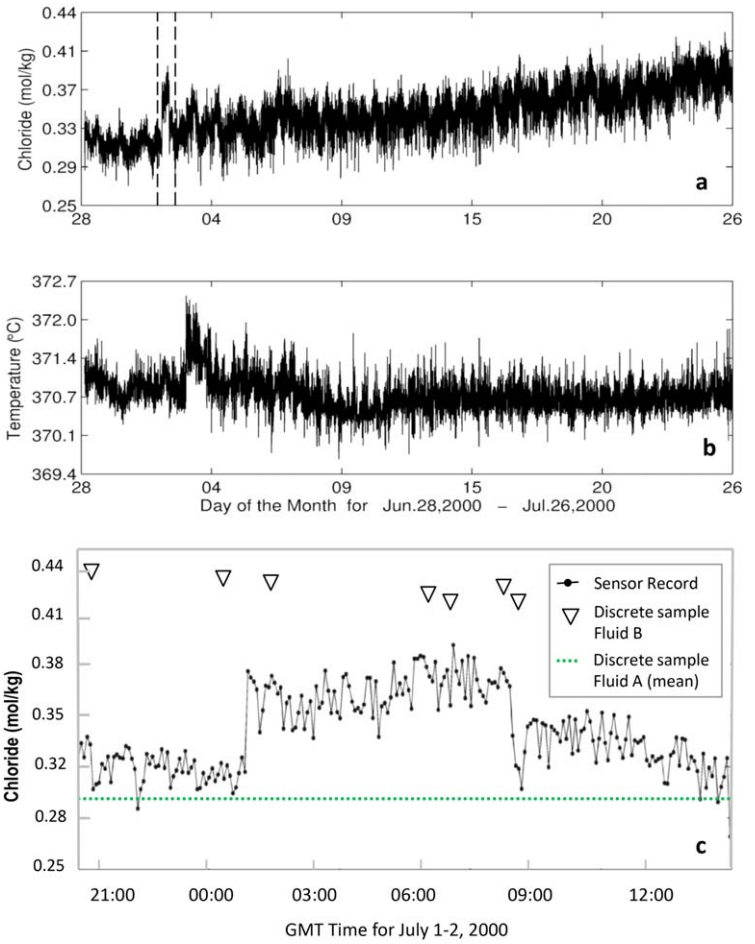

Figure 2. Chloride (a) and Temperature (b) data at the Sully structure collected with an in situ sensor, showing a positive excursion in both parameters lasting about 7 hours during the time that the samples on 1 and 2 July (fluid B) were collected. (c) A detail view of the resistivity based chloride data during the period indicated by vertical dashed lines in Figure 2a. The discrete samples are shown by the triangle symbols. The horizontal dashed line represents the average chloride of fluid A discrete samples from the days prior to this time period.

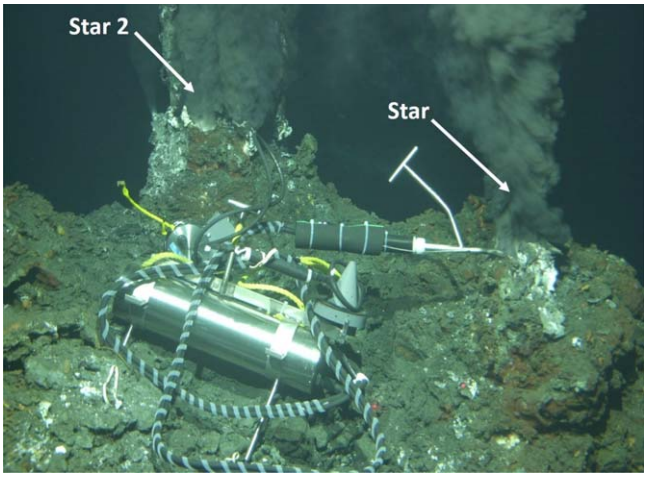

Figure 3. Sully structure at the time of sampling. Most samples collected from group of orifices at the star and star 2 locations, as indicated in the image (see Supporting information Table S2 for specific samples and locations). The Spider orifice is located about 2 m lower on the structure.

NaCl was used to determine the relative amounts of each phase.

3. Data

The chloride and volatile concentrations of samples collected at Sully over several days in late June and early July of 2000 are presented in Figure 1 and Supporting information Tables S1 and S2. Fluid composition was relatively stable throughout the sampling period and between locations on the structure (fluid A) except for 1 July, when chloride increased by approximately 50% and gas content decreased by about 50% (fluid B). A resistivity probe deployed at Sully registered this change, which lasted for 7 hours in the sensor record (Figure 2). Two of the discrete samples corresponding to fluid B were collected before the start of the excursion in the sensor record. This difference between the two records may be due in part to spatial variability on the structure. The first two discrete samples were collected from the spider orifice, which was located lower on the structure than the star marker where the sensor was deployed and where some of the later fluid B samples were collected (Supporting information Table S2, Figure 3). The magnitude of the change in chloride measured by the resistivity probe was also somewhat smaller than that measured in the discrete samples. The fluid chemistry measured in the discrete samples is more robust and is used for all calculations here.

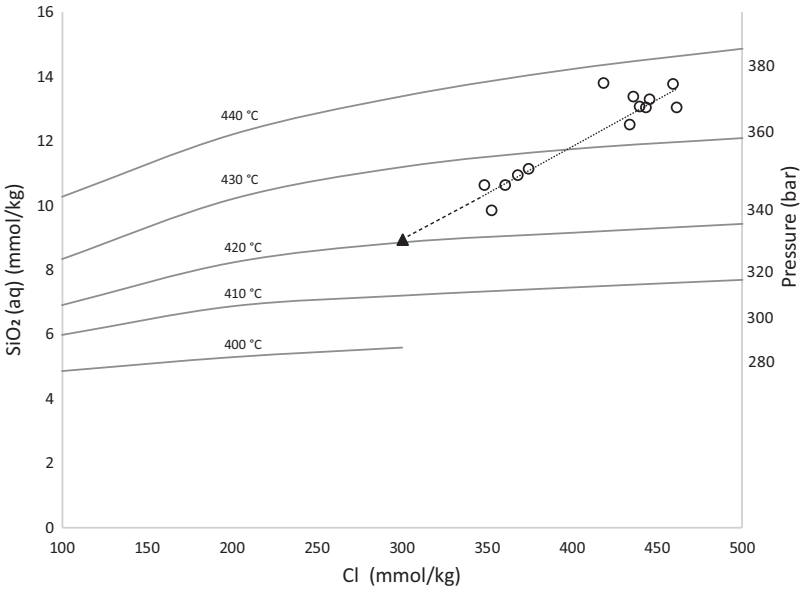

Figure 4. Quartz solubility curves generated from the equations of Foustoukos and Seyfried [2007b] as compared to measured silica concentration in fluids from the Sully structure. The dotted line is a linear extrapolation indicating the likely silica concentration of fluid A (black triangle). Samples with chloride between 350 and 400 mmol/kg do not have associated volatile data.

The resistivity probe also measured a slow increase in chloride with respect to the pre-offset conditions over the next 10 weeks [*Larson et al*., 2009] (Figure 2). This long-term change can also be seen in the discrete samples collected in September (Supporting information Tables S1 and S2). Silica, was also measured in fluid B and other associated samples from Sully on the same day with intermediate chloride content (Supporting information Table S3). Unfortunately, these data are not available for the fluid A samples. However, other samples collected at this structure during the same time period exhibit a linear trend of silica with chloride which can be used to estimate a Si content for fluid A (Figure 4). Iron and magnesium were measured on samples collected at Sully in 2000 for which gas data are not available (Supporting information Table S3). Both the short and long term variability in fluid composition at Sully may be related to the reorganization of the system following seismic disturbances in 1999 [*Lilley et al*., 2003; *Seyfried et al*., 2003].

4. Discussion of Scenarios

4.1. Conditions of Phase Separation

Every explanation for the presence of these disparate fluids at the sully structure depends on phase separation. Therefore, it is critical to establish the potential temperature and pressure conditions for this process. In the simplest model for hydrothermal circulation at MEF, seawater enters the crust, penetrates downward into a deep reaction zone where it is heated, and its chemistry modified through fluid/rock interactions. As it begins to become buoyant, the fluid encounters the two phase curve. When brine condensation occurs, some phase segregation is commonly assumed, and while brine accumulates in the crust, the vapor rises to eventually emerge at the sea floor with little change to the chloride concentration of the fluid as it rises.

The Fe/Mn geothermometer of Pester et al. [2011] uses experimentally derived Fe and Mn concentrations of fluids in equilibrium with basalt to formulate a log linear relationship between the elemental ratio of Fe/Mn and temperature. The ratios from fluids at Sully in 2000 indicate a temperature of equilibration of 405 $\pm$ 2°C. Other estimates vary, including phase separation temperatures of less than 420°C estimated for MEF based on volatile partitioning [*Seewald et al*., 2003]. Reaction zone conditions based on mineral-fluid equilibria gave a range of 375–400°C and 300–350 bar [*Seewald et al*., 2003; *Seyfried et al*., 2003]. If we assume that fluid A (303 mmol/kg Cl) is the vapor phase, relatively unchanged since deep brine condensation, and chose conditions consistent with this range of estimates for T and P conditions, then it could be produced by phase separation at 410°C, 304.1 bar [*Driesner and Heinrich*, 2007a, 2007b]. The pressure of 304.1 bar corresponds to a depth of at least 700 m below the seafloor, given that the seafloor depth is close to 2200 m at

the Sully structure [*Kelley et al*., 2012]. This is not a unique solution, but one of many temperature and pressure conditions that could produce a vapor of this composition.

Alternatively, we could estimate the conditions in the reaction zone by examining the silica concentration in the fluids with respect to quartz equilibrium. The solubility of silica in hydrothermal fluids and its utility when combined with chloride as a geobarometer has been investigated and applied in several studies [e.g., *Wells and Ghiorso*, 1991; *Foustoukos and Seyfried*, 2007b; *Fontaine et al*., 2009, and references therin], including estimates for the MEF [*Fontaine et al*., 2009]. Silica data for samples collected at the Sully structure in 2000 indicate potential reaction zone conditions of between 420 and 440°C and 340–380 bar when compared to quartz solubility curves (Figure 4). There are several additional caveats that must be considered when using quartz solubility to estimate reaction zone depth, including the effects of mixing, temperature gradients, chloride variability, and flow rates. However, the depth of circulation estimated with this method over a range of vent fields compares well to the depth of magma chambers measured with geophysical imaging, suggesting a measure of confidence in the Si-Cl geobarometer [*Fontaine et al*., 2009]. Given these estimates, fluid A could also be the vapor produced by brine condensation at for instance, 430°C and 352 bar. The Si-Cl geobarometer does estimate higher temperatures than the Fe/Mn geothermometer. Given the lack of complete information about subsurface mixing processes, residence time, reactions rates, and fluid composition, it is impossible to determine why the estimates do not match, nor determine which is more accurate. We therefore investigate a range of possibilities encompassed by these estimates.

4.2. A Change in the Conditions of Phase Separation

One possible explanation for the short-term variability is that the conditions of phase separation (temperature and pressure) changed, causing a shift in the composition of the vapor phase fluid venting at the seafloor. From either of the starting points outlined in section 4.1, the changes in chloride at Sully (from 303 to 440 mmol/kg) could be accommodated by small changes in the temperature (<2°C) or pressure (<4 bar) conditions of phase separation. However, the changes in volatile concentrations cannot be explained by this mechanism (Figure 5a) because volatile enrichment is relatively insensitive to the amount of condensed brine retained at depth. Although the direction of change in volatile concentration brought about by these changes would be in the same direction as those observed, the magnitude of the changes make this scenario unlikely. The mass of brine produced changes by only about 8–10%, and brines remain saline enough (more than twice seawater salinity) to keep gas solubility quite low. Volatiles are expected to partition preferentially into the vapor phase in this situation, therefore a small change in the mass of brine, which will have low volatile content, cannot produce a 50% change in volatile concentrations in the vapor as would be required in this scenario. This would be true for a range of initial conditions for production of fluid A as a vapor conjugate produced during brine condensation.

In addition, if both fluids are the vapor produced by brine condensation of hydrothermal source fluid, then the argon concentrations observed in these samples cannot be reconciled. Argon concentrations in hydrothermal fluid should be influenced primarily by phase separation. If these fluids are vapors produced in a single pass system, then the argon concentration in the vapor phase must always be equal to or greater than the seawater concentration. In the Sully samples, argon concentrations are close to the background seawater value in the lower chloride fluids (fluid A). This observed argon concentration is also very close to the 0.01615 mmol/kg solubility value for argon at 2°C and salinity of 35 [*Hamme and Emerson*, 2004]. Argon concentration is about 50% of the seawater value in the higher chloride fluids (fluid B). Therefore, fluid B cannot be produced as a vapor phase arising from a seawater salinity hydrothermal source fluid.

One can examine the interplay between changes in different parameters as well. Both chloride and argon concentrations are significantly lower in Fluid B than in seawater. Phase separation should cause opposite trends in these parameters. This simple model of one phase separation event followed by venting of the vapor phase can be ruled out for these fluids.

4.3. Mixing Scenarios

Given the estimated reaction zone conditions from the quartz solubility data, brine condensation is a likely mode of phase separation. Fluid A could be produced under these conditions, along with a relatively high salinity brine as described above. Mixing of fluid A with a brine can produce the required changes in chloride, but cannot produce the observed changes in gas content in fluid B. This is because so little brine is

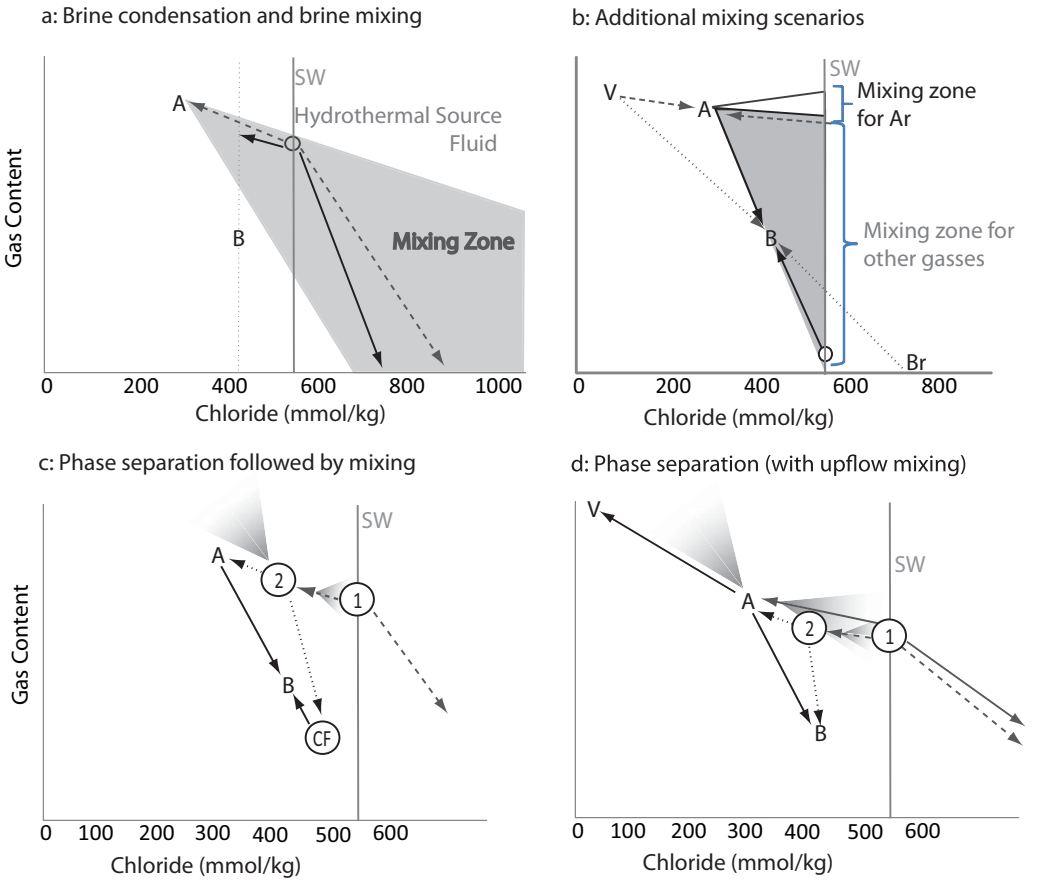

Figure 5. (a) How neither mixing fluid A with a high salinity brine (which would produce fluids in the shaded area) nor a change in the conditions of brine condensation (shift from compositions indicated by the dashed arrows to the solid arrows) can produce both fluids A and B. (b) The mixing zone between fluid A and a relatively unconstrained hydrothermal source fluid (shaded area, mixing represented by solid lines), and the mixing zone specific to argon, which does not encompass fluid B. Also depicted is a low salinity vapor (V) which can produce A when mixed with hydrothermal source fluid (dashed lines) and B when mixed with a relatively low salinity brine (dotted lines). (c) How fluid B can be produced through the mixing of fluids produced by near critical phase separation (mixing indicated by solid lines). Shaded areas indicate potential mixing of vapor and hydrothermal source fluids in the upflow zone. CF is the conjugate fluid of A. Dotted lines indicate the second phase separation and dashed lines indicate the first phase separation. (d) A scenario in which fluid A is the vapor produced by brine condensation and fluid B is the liquid phase produced from it along with a low salinity vapor (solid grey arrows and black arrows). Shaded areas indicate potential mixing of vapor, brine, and hydrothermal source fluids in the upflow zone. Also shown in Figure 5d. Fluids A and B may be a conjugate pair themselves, produced by phase separation of a vapor phase fluid. Dotted lines indicate the second phase separation and dashed lines indicate the first phase separation.

required to produce the chloride changes, that the dilution of the existing gas content is small. Mass balance calculations show that even a relatively low salinity brine with zero gas content cannot produce the relatively large observed changes in volatile concentrations. This is illustrated in Figure 5a, where the shaded area indicates the fluids that can be produced by mixing of fluid A with moderate to high salinity brines. The composition of fluid B is outside of this mixing zone. Two phase fluid flow models also indicate that in general, high salinity brines are not very mobile in these systems, further reducing the likelihood of this mechanism [*Coumou et al*., 2009; *Singh et al*., 2013; *Weis et al*., 2014].

Another mixing scenario that must be considered is mixing with hydrothermal source fluids. These are hydrothermal fluids of seawater salinity which have been modified through fluid rock interactions and/or magmatic influence, but have not undergone phase separation (Figure 5b). A mixture of fluid A composition with an approximately equal quantity of seawater salinity fluid could produce the observed chloride change in fluid B. This hydrothermal source fluid would need to have acquired slightly elevated concentrations of CO_2, CH_4, H_2, and H_2S, in order for the mixture to obtain the measured concentrations of these gasses (indicated by the open circle in Figure 5b). This could be achieved through water rock reactions and magmatic input without phase separation. This explanation does require strong enrichment in gasses in fluid A over

the hydrothermal source fluid which is unlikely when brine condensation is the dominant mode of phase separation. The line of reasoning which precludes this mixing scenario for fluids A and B is that it would require an Ar concentration of only 20% of the background seawater concentration in the hydrothermal source fluid. Ar is generally nonreactive and there is no obvious mechanism by which it could be removed from a seawater-like fluid other than through phase separation.

A more likely range of argon in the hydrothermal source fluid is depicted in Figure 5b, indicating that the modest range of Ar is expected in these non-phase separated fluids source fluids, centering around the measured ambient seawater value in the deep water at the MEF of 0.016 mmol/kg. The resultant mixing zone does not encompass fluid B. While mixing of a moderate salinity vapor produced by brine condensation with hydrothermal source fluid cannot have produced fluids A and B, these data do not rule out this mechanism to explain other fluids at MEF that were only modestly depleted in chloride [*Seyfried et al*., 2003]. The data do however, highlight the utility of argon in the interpretation of such fluids.

Most numerical models of similar systems do indicate significant mixing of vapor phase fluids with hydrothermal source fluid, though limited in some cases by anhydrite mineral precipitation around upflow zones [*Coumou et al*., 2009; *Singh et al*., 2013]. Much lower salinity vapors (approximately 0.5 wt % NaCl, or about 75 mmol Cl/kg) may be prevalent in the reaction zone at MEF (Singh, 2013). If this is the case, then such a vapor (V) could mix with hydrothermal source fluid to produce fluid A, however this vapor would need to have an Ar concentration close to the nominal source fluid (Figure 5b). Under the conditions predicted by quartz solubility (about 430°C, 350 bar) the brines produces are about 3 times seawater salinity and the vapors could exhibit very low gas enrichment. Fluid B could then also be produced by a mixture of this vapor (V) with a relatively low salinity brine. Assuming no argon in the brine, a mass balance calculation for argon and chloride indicates that the brine must have a maximum salinity of 5.2 wt % NaCl, or 817 mmol/kg Cl. This is much lower in chloride than most brines that are expected to be produced in the MEF (Singh, 2013) and much lower in chloride than the conjugate pair of the vapor in question. This unlikely mixing scenario would require a transient and unknown mechanism to initiate brine mixing without significant dilution by hydrothermal source fluid in the upflow zone (which would bring the argon concentrations up again).

4.4. Near Seafloor Phase Separation

If the variation observed at Sully is the result of partial remixing or incomplete phase segregation of fluids produced in the shallow subsurface, little to no cooling would be expected, putting the conditions at about 380°C and about 225 bar. There would be no time for fluids to equilibrate with mineral assemblages, including quartz, so these conditions would not be reflected in the quartz solubility. This would produce a very low chloride vapor phase (~10 mmol Cl/kg), and a brine with about two times seawater salinity. While incomplete phase segregation of these fluids can produce fluids with the chloride content of fluids A and B, they cannot produce the large variation in gas content, regardless of gas partitioning. In this case, the vapor that is produced is highly enriched in volatiles given the expected range of gas partitioning, similar to V in Figure 5d. The proportion of brine that would be needed to generate the observed change in chloride is about 30% in the case of fluid A and 50% in the case of fluid B, so enrichment in gas content of fluid A over fluid B cannot be more than 30% regardless of gas partitioning, as compared to the 100% enrichment observed. In addition, the argon content of fluid B does not lie inside the field of possible compositions for a three component mixture of this vapor, brine, and a hydrothermal source fluid of seawater salinity and argon concentration close to the saturated seawater value. Therefore, phase separation at or very near the seafloor cannot have produced these fluids.

If the depth of phase separation is somewhat deeper, with a pressure of about 231 bar (or about 50 mbsf), and still with a temperature of 380°C, then the vapor produced is still very low in chloride (17 mmol/kg), however the higher salinity fluid matches the chloride content, and potentially the gas content of fluid B. In this case, fluid A is similar in argon and chloride content to a 2:1 mixture of the two phases. When the rising fluid encountering the two-phase region has a chloride content of 300 mmol/kg then fluid A is also the same as a completely non-phase segregated fluid (Figure 5d, black arrows). Volatility ratios cannot be estimated in this case because the vapor phase was not sampled. Since both fluids have salinities less than sea water, this scenario does require two zones of phase separation as suggested in modeling results from Coumou et al. (2009)—a deeper brine condensation zone, from which the vapor phase rises, perhaps mixing with non-phase separated hydrothermal source fluid, to encounter a zone of boiling. The critical

Table 1. Measured Concentrations of Chloride and Volatiles in mmol/kg Are Shown for Fluid A and Fluid B at Sully

	Cl	CO_2	CH_4	H_2S	H_2	Ar
Fluid A (vapor)	303	29	0.90	14	0.30	0.016
Fluid B (liquid/mixture)	448	15	0.64	7	0.14	0.008
Conjugate (calculated)	484	11	0.58	5	0.10	0.006
Log K_D mixing model		0.40	0.30	0.42	0.48	0.43
Log K_D conjugate pair model		0.28	0.19	0.30	0.33	0.30

[a]The theoretical conjugate fluid that could produce the 448 mmol/kg fluid if mixed in an 80/20 ratio with the vapor is also shown. These values are calculated as follows: $Conjugate = \frac{Fluid\ \ B - (0.2\ \ Fluid\ \ A)}{0.8}$, $K_D = \frac{moles\ \ gas\ \ vapor}{moles\ \ water} / \frac{moles\ \ gas\ \ in\ \ conjugate}{moles\ \ water}$. For the mixing model, the conjugate is the calculated fluid. For the Conjugate Pair model, it is fluid B.

pressure at this temperature is 235 bar, and the fractions of the two phases produced are similar, indicating that these conditions are near critical.

4.5. Multiple Phase Separation Plus Mixing

If fluid A is assumed to be the pure vapor phase fluid, and the temperature of phase separation is 404°C, in accordance with the Fe/Mn estimates, the conjugate pair of this fluid has 484 mmol/kg Cl and phase separation occurs near 290.6 bar (about 500 mbsf). These conditions are very close to the critical point, which is at 291°C bar for 404° fluid [*Bischoff and Pitzer*, 1989; *Driesner and Heinrich*, 2007]. The fluid source for this conjugate pair must, again, have lower than seawater chloride content arising from previous phase separation, likely brine condensation, potentially followed by mixing with hydrothermal source fluids. If phase segregation is not complete, a mixture of 80% higher chloride phase with 20% vapor phase will produce the observed chloride concentrations during this high chloride excursion (fluid B).

For a temperature range of 400–410°C, this second phase boundary encounter would occur between about 800 and 450 m below the seafloor. To put these depths in their geophysical context, Van Ark et al. [2007] found evidence of a crustal magma chamber beneath the MEF at a depth of about 2.1 km. Further studies indicate that a zone of higher seismic velocities, which may indicate lower porosity because of precipitation of hydrothermal minerals, is found at depths of about 1000–1500 m below the sea floor, while a zone of more intense seismicity is found just above the axial magma chamber [*Wilcock et al.*, 2009; *Weekly et al.*, 2014].

Based on the mixing ratio calculated from a mass balance for salinity, the volatile concentrations in the conjugate fluid can be calculated such that mixing with the vapor will produce the observed volatile concentrations. These values are listed in Table 1 along with the apparent gas partition coefficients they imply, where K_D is the ratio of the mole fraction of gas in the vapor phase to that in the brine or liquid phase. The phase separation conditions and mixing ratio upon which these estimates are based are simply an example of one possible origin for these fluids. Therefore, these partition coefficients provide context for the relative merits of these scenarios when compared to theoretical values, but are not intended to be true measurements of gas partitioning in near critical fluids.

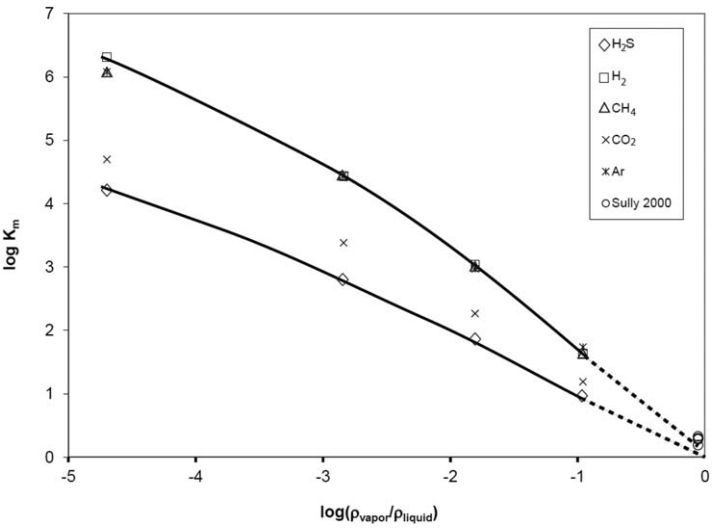

Figure 6. The partition coefficients from Fernandez-Prini et al. (2003) are shown for several gasses. Solid lines indicate the P-T region in which these measurements were taken. Data have not been gathered close to the critical point, but at the critical point the K_D must equal 1. Dotted lines indicate the extrapolation towards this theoretical value. Values calculated from the conjugate pair model are shown as circles, and lie very close to the critical point, and near the range of expected values.

There have been few investigations of volatility ratios at high temperature and in saline fluids, and existing studies do not include data close to the critical point, with the exception of some experimental data particularly for H_2 and H_2S [*Drummond*, 1981; *Drummond and Ohmoto*, 1985; *Fernandez-Prini et al.*, 2003; *Foustoukos and Seyfried*, 2007a]. A comparison to theoretical partition coefficients is therefore only approximate. Fortunately, the partitioning of volatiles can be described as simple functions relative to the

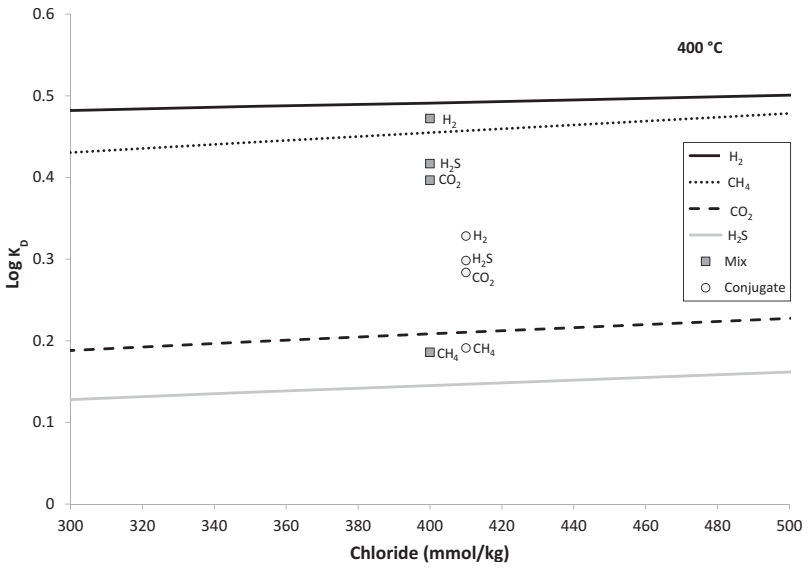

Figure 7. The apparent partition coefficient (K_D) estimated from this work compared to linear estimates of Drummond [1981] (Shown as lines) as a function of the chloride content of the water at 400°C. This close to the critical point these linear estimates are extrapolations from measured data. K_D values are calculated based on K_H values and fluid properties. Chloride assigned to each model is arbitrary, because bulk salinity influences the proportions but not the composition of the two resulting fluids in the two phase region. Assigned values are within the range that would produce significant quantities of both phases during near critical phase separation. The mixing model better reproduces the range of expected K_D values, and both models show the apparent partitioning of H_2S into the vapor phase is higher than expected relative to other gasses.

log of the ratio of the density of the two fluids, which allows for a rough comparison of fluids of differing bulk salinities. This comparison is presented in Figure 6, where the fresh water values of Fernandez-Prini et al. [2003] show the general shape of these curves over a large temperature range. The curves for seawater are similar but data for argon are not available. The partition coefficients calculated based on this mixing scenario do fall close to these estimates. The K_D values which are slightly higher than predicted may be due to salting out effects relative to the fresh water values used to create these curves. The partition coefficients presented in Drummond (1981, 1985) can also provide context for our estimates. A comparison of K_D values with data for water of similar salinity is presented in Figure 7. Linear estimates for these extrapolations may break down close to the critical point, and given the uncertainties and extrapolation necessary to make these estimates, the mixing model matches these predicted values relatively well. This model indicates that H_2 partitions most strongly into the vapor phase. This is consistent with theoretical estimates (Figures 6 and 7), and with the theoretical framework and results from laboratory studies of two phase fluids and fluid-mineral equilibria [*Foustoukos and Seyfried*, 2007a]. Calculated partition coefficients for H_2S which are higher than predicted could be due to fluid rock equilibrium effects overprinting the phase separation signature. Previous work has shown that fluids at the MEF in 1999 and 2000 showed evidence of control of H_2 and H_2S by fluid rock equilibrium at near critical conditions (about 410° and 300 bar) and re-equilibration and/or mixing in the upflow zone for some structures, [*Seewald et al*., 2003; *Seyfried et al*., 2003].

Apparent volatile partitioning as compared to theoretical values does not rule out either the mixing model or conjugate pair model. Uncertainty in the phase separation conditions used to generate these estimates, proximity of the proposed conditions for this model to the critical point and likely nonlinear effects in this pressure temperature region make further detailed interpretation of partition coefficients unwarranted.

This scenario does require a specific mixing ratio of the two fluids to be present across several hours, and an abrupt transition to no mixing at all on the days preceding and following. This scenario may be supported by the sensor record which does display some high and moderate frequency variability in the chloride record which could indicate greater variability in the mixing ratio and therefore the fluid chemistry, than that captured in the discrete samples. Samples of intermediate salinity were also captured interspersed with those matching fluid B in bottles analyzed for silica, but not for volatiles (Supporting information Table S3).

4.6. Observed Fluids Are Conjugate Pair

Perhaps the simplest explanation of these observations is that the two fluids described here are themselves a conjugate pair, produced by phase separation of a moderate salinity vapor (produced by brine condensation) in the shallow subsurface (Figure 5d). Conditions of 403° and 288.33 bar (approximately 650 mbsf) produce two fluids which match the chloride content of those observed at Sully. Partition coefficients of the volatile components can be calculated in this case, and these values are similar to those calculated for the phase separation and mixing scenario, and to those estimated theoretically (Table 1, Figures 6 and 7).

While near sea floor phase separation is probably not a force driving larger scale patterns observed at MEF [*Butterfield et al*., 1994; *Seewald et al*., 2003], it should be noted that some data of Butterfield et al. [1994] do indicate the influence of boiling of fluids after brine condensation. Previous data do not rule out the influence of near sea floor phase separation on small spatial scales, but do indicate that this kind of phase separation cannot explain the data in the absence of brine condensation. The scenario described here also requires a zone of deep brine condensation which produces a fluid of bulk salinity between the compositions of fluid A and B which are both less than seawater salinity. The model of Coumou et al. (2009) suggests the possibility of just such a zone, above which the vapor mixes with non-phase separated fluids to form an upflow zone with fluid of approximately 2 wt % NaCl. Fluid A (1.8 wt %) and fluid B (2.6 wt %) could be produced by near critical phase separation of such a fluid.

If near-sea floor phase separation were common, it would be expected that the conjugate fluids produced would be periodically observed, which has not been the case. These fluids would be expected to have a salinity only moderately greater than or less than seawater values, depending on the P-T conditions and bulk salinity of the rising fluids. It is possible that temporal and spatial variability in the release of these fluids has obscured their presence previously or that this type of phase separation is a transient feature.

This conjugate pair scenario would require little to no mixing during the final ascent of these fluids. The existence of a low permeability shell around areas of high temperature discharge, attributed to precipitation of anhydrite was suggested by Cann and Strens [1989] among others, and is necessary to resolve numerical model results given the otherwise high permeability of layer 2a [*Wilcock*, 1998; *Singh et al*., 2013]. High resolution magnetic data give some support to this idea as well [*Tivey and Johnson*, 2002]. These low permeability barriers would limit heat loss and mixing with seawater in layer 2A as the fluids approach the seafloor, however this barrier would not impede mixing of the two phases as they ascend.

5. Conclusions

The three scenarios which include deep brine condensation followed by potential mixing in the upflow zone, and near critical phase separation closer to the sea floor (Figures 5c and 5d) provide the most plausible explanations for the variations in chlorinity and gas content observed at Sully in June/July of 2000. These samples may represent (1) the vapor produced by deep brine condensation and mixing in the upflow zone (fluid A) and the liquid produced from it upon near critical phase separation (fluid B), (2) a near critical conjugate pair, or (3) the vapor and a mixture of the two phases resulting from near critical phase separation. Quartz and basalt equilibrium data do not rule out any of these models. The fluids of moderate, less than seawater salinity, or the vapor and brines required as inputs in these scenarios can be generated under higher temperature reaction zone conditions from the quartz geobarometer, perhaps with mixing of hydrothermal source fluids. The temperatures for both the mixing and conjugate pair models match estimates from the Fe/Mn geothermometer (403 and 404 vs. 405°C).

These analyses corroborate certain aspects of recent modeling results for phase separation at MEF [*Singh et al*., 2013] or in hydrothermal systems with pressure-temperature conditions similar to MEF [*Coumou et al*., 2009] and add to the limited data available on gas partitioning close to the critical point. Where field results from MEF have been examined in light of vapor partitioning, they indicate that phase separation conditions between 400 and 410°C, close to the critical temperature for seawater, bracket the likely conditions producing fluids of a similar salinity to those observed here [*Seewald et al*., 2003]. These conditions encompass two of the more detailed scenarios suggested by our data from Sully. The range of K_D values estimated in both these models (K_D of about 1–4) are similar to those estimated using available experimental data (Figures 6 and 7).

A better understanding of real phase separation events in hydrothermal systems leads to better interpretations of fluid chemistry and improved understanding of variability in these systems, which has not been widely captured before by discrete sampling. With the advent of cabled observatories providing long-term and real-time data for a limited set of hydrothermal properties (e.g., salinity and temperature) from hydrothermal sensors, it is critical to use more multi-dimensional datasets, such as that presented in this paper, to help determine which models can best explain the observed variability. Our analysis of high-frequency sampling for volatiles highlights the importance of developing in situ sensors capable of monitoring gas concentrations simultaneously with other properties. We do not suggest that these data are broadly representative of the MEF, but rather present them as an example of the detailed analysis which is possible when high resolution volatile sampling captures variable geochemical conditions.

Acknowledgments

Data supporting this work and these conclusions can be found in the tables in the supporting information and in the references. The authors are not aware of any conflicts of interest. We gratefully acknowledge the contributions of the officers and crew of the R/V Atlantis, the Alvin group, sample analysis by Kevin Roe and thoughtful input from our reviewers. Funding for this work provided through: National Science Foundation Award numbers OCE-9911879, OCE-9904396, and OCE-0085615. This work is also partially funded by the W.M. Keck Foundation gift for Project NEPTUNE and by the Joint Institute for the Study of the Atmosphere and Ocean (JISAO) under NOAA Cooperative Agreement NA10OAR4320148 (2010–2015) and NA15OAR4320063 (2015–2020). This is JISAO contribution 2016-01-32, and PMEL contribution 4530.

References

Barreyre, T., J. Escartín, R. Sohn, M. Cannat, V. Ballu, and W. C. Crawford (2014), Temporal variability and tidal modulation of hydrothermal exit-fluid temperatures at the Lucky Strike deep-sea vent field, Mid-Atlantic Ridge, *J. Geophys. Res. Solid Earth*, *119*, 2543–2566, doi:10.1002/2013JB010478.

Berndt, M. E., M. E. Person, and W. E. Seyfried (2001), Phase separation and two-phase flow in seafloor hydrothermal systems, in *11 ANN VM GOLDSCHM C*.

Bischoff, J. L., and R. J. Rosenbauer (1985), An empirical equation of state for hydrothermal seawater (3.2 percent NaCl), *Am. J. Sci.*, *285*(8), 725–763.

Bischoff, J. L., and R. J. Rosenbauer (1987), Phase-separation in seafloor geothermal systems—An experimental study of the effects on metal transport, *Am. J. Sci.*, *287*(10), 953–978.

Bohnenstiehl, D. R., R. P. Dziak, M. Tolstoy, C. G. Fox, and M. Fowler (2004), Temporal and spatial history of the 1999-2000 Endeavour Segment seismic series, Juan de Fuca Ridge, *Geochem. Geophys. Geosyst.*, *5*, Q09003, doi:10.1029/2004GC000735.

Butterfield, D., R. McDuff, M. Micheal, M. D. Lilley, J. E. Lupton, and G. Massoth (1994), Gradients in the composition of hydrothermal fluids from the Endeavour segment vent field: Phase separation and brine loss, *J. Geophys. Res.*, *99*(B5), 9561–9583.

Butterfield, D. A., K. K. Roe, M. D. Liley, J. A. Huber, J. A. Baross, R. W. Embley, and G. J. Massoth (2004), Mixing, reaction and microbial activity in the sub-seafloor revealed by temporal and spatial variation in diffuse flow vents at axial volcano, in *The Subseafloor Biosphere at Mid-Ocean Ridges*, edited by W. Wilcock, E. DeLong, D. Kelley, J. Baross, and C. Car, 408 pp., AGU, Washingdon, D. C.

Cann, J. R., and M. R. Strens (1989), Modeling periodic megaplume emission by black smoker systems, *J. Geophys. Res.*, *94*(B9), 12,227–12,237, doi:10.1029/JB094iB09p12227.

Coumou, D., T. Driesner, P. Weis, and C. A. Heinrich (2009), Phase separation, brine formation, and salinity variation at black smoker hydrothermal systems, *J. Geophys. Res.*, *114*, B03212, doi:10.1029/2008JB005764.

Crone, T. J., and W. S. D. Wilcock (2005), Modeling the effects of tidal loading on mid-ocean ridge hydrothermal systems, *Geochem. Geophys. Geosyst.*, *6*, Q07001, doi:10.1029/2004GC000905.

Driesner, T., and C. A. Heinrich (2007a), The system H2O-NaCl. Part I: Correlation formulae for phase relations in temperature-pressure-composition space from 0 to 1000 degrees C, 0 to 5000 bar, and 0 to 1 X-NaCl, *Geochim. Cosmochim. Acta*, *71*(20), 4880–4901, doi:10.1016/i.gca.2006.01.033.

Driesner, T., and C. A. Heinrich (2007b), The system H2O-NaCl. Part II: Correlations for molar volume, enthalpy, and isobaric heat capacity from 0 to 1000 degrees C, 1 to 5000 bar, and 0 to 1 X-NaCl, *Geochim. Cosmochim. Acta*, *71*(20), 4902–4919, doi:10.1016/j.gca.2007.05.026.

Drummond, S. (1981), Boiling and mixing of hydrothermal fluids: Chemical effects on mineral precipitation, PhD dissertation, Pa. State Univ., State College.

Drummond, S. E., and H. Ohmoto (1985), Chemical evolution and mineral deposition in boiling hydrothermal systems, *Econ. Geol.*, *80*, 126–147.

Edmond, J. G. (1992), Submersible-deployed samplers for axial vent waters, in *Ridge Events*, vol. 3, pp. 23–24.

Fanning, K. A., and M. E. Q. Pilson (1973), On the spectrophotometric determination of dissolved silica in natural waters., *Anal. Chem.*, *45*(1), 136–140, doi:10.1021/ac60323a021.

Fernandez-Prini, R., J. L. Alvarez, and A. H. Harvey (2003), Henry's constants and vapor-liquid distribution constants for gaseous solutes in H_2O and D_2O at high temperatures, *J. Phys. Chem. Ref. data*, *32*(2), 903–916, doi:10.1063/1.1564818.

Fontaine, F. J., and W. S. D. Wilcock (2006), Dynamics and storage of brine in mid-ocean ridge hydrothermal systems, *J. Geophys. Res.*, *111*, B06102, doi:10.1029/2005JB003866.

Fontaine, F. J., W. S. D. Wilcock, D. E. Foustoukos, and D. A. Butterfield (2009), A Si-Cl geothermobarometer for the reaction zone of high-temperature, basaltic-hosted mid-ocean ridge hydrothermal systems, *Geochem. Geophys. Geosyst.*, *10*, Q05009, doi:10.1029/2009GC002407.

Foustoukos, D. I., and W. E. Seyfried (2007a), Fluid phase separation processes in submarine hydrothermal systems, *Rev. Mineral. Geochem.*, *65*(1), 213–239, doi:10.2138/rmg.2007.65.7.

Foustoukos, D. I., and W. E. Seyfried (2007b), Quartz solubility in the two-phase and critical region of the NaCl-KCl-H2O system: Implications for submarine hydrothermal vent systems at 9 degrees 50'N East Pacific Rise, *Geochim. Cosmochim. Acta*, *71*(1), 186–201, doi:10.1016/j.gca.2006.08.038.

Foustoukos, D. I., N. J. Pester, K. Ding, and W. E. Seyfried (2009), Dissolved carbon species in associated diffuse and focused flow hydrothermal vents at the Main Endeavour Field, Juan de Fuca Ridge: Phase equilibria and kinetic constraints, *Geochem. Geophys. Geosyst.*, *10*, Q10003, doi:10.1029/2009GC002472.

Gruen, G., P. Weis, T. Driesner, C. A. Heinrich, and C. E. J. de Ronde (2014), Hydrodynamic modeling of magmatic–hydrothermal activity at submarine arc volcanoes, with implications for ore formation, *Earth Planet. Sci. Lett.*, *404*, 307–318, doi:10.1016/j.epsl.2014.07.041.

Hamme, R. C., and S. R. Emerson (2004), The solubility of neon, nitrogen and argon in distilled water and seawater, *Deep Sea Res. Part I Oceanogr. Res. Pap.*, *51*(11), 1517–1528, doi:10.1016/j.dsr.2004.06.009.

Han, L., R. P. Lowell, and K. C. Lewis (2013), The dynamics of two-phase hydrothermal systems at a seafloor pressure of 25 MPa, *J. Geophys. Res. Solid Earth*, *118*, 2635–2647, doi:10.1002/jgrb.50158.

Johnson, H., M. Hutnak, R. Dziak, C. Fox, I. Urcuyo, J. Cowen, J. Nabelek, and C. Fisher (2000), Earthquake-induced changes in a hydrothermal system on the Juan de Fuca mid-ocean ridge, *Nature*, *407*(6801), 174–177, doi:10.1038/35025040.

Kelley, D. S. D., et al. (2012), Endeavour segment of the Juan de Fuca Ridge: One of the most remarkable places on earth, *Oceanography*, *25*(1), 44–61, doi:10.5670/oceanog.2012.03.

Larson, B. I., M. D. Lilley, and E. J. Olson (2009), Parameters of subsurface brines and hydrothermal processes 12-15 months after the 1999 magmatic event at the Main Endeavor Field as inferred from in situ time series measurements of chloride and temperature, *J. Geophys. Res.*, *114*, B11201, doi:10.1029/2008JB005627.

Lilley, M. D., D. A Butterfield, J. E. Lupton, and E. J. Olson (2003), Magmatic events can produce rapid changes in hydrothermal vent chemistry, *Nature*, *422*(6934), 878–881, doi:10.1038/nature01569.

Mittelstaedt, E., D. J. Fornari, T. J. Crone, J. Kinsey, and D. Kelley (2016), Diffuse venting at the ASHES hydrothermal field: Heat flux and tidally modulated flow variability derived from in situ time-series measurements, *Geochem. Geophys. Geosyst.*, *17*, 1435–1453, doi:10.1002/2015GC006144.

Pester, N. J., M. Rough, K. Ding, and W. E. Seyfried (2011), A new Fe/Mn geothermometer for hydrothermal systems: Implications for high- salinity fluids at 13° N on the East Pacific Rise, *Geochim. Cosmochim. Acta*, *75*(November 2016), 7881–7892, doi:10.1016/j.gca.2011.08.043.

Seewald, J., A. Cruse, and P. Saccocia (2003), Aqueous volatiles in hydrothermal fluids from the Main Endeavour Field, northern Juan de Fuca Ridge: Temporal variability following earthquake activity, *Earth Planet. Sci. Lett.*, *216*(4), 575–590, doi:10.1016/S0012-821X(03)00543-0.

Seyfried, W. E., J. S. Seewald, M. E. Berndt, K. Ding, and D. I. Foustoukos (2003), Chemistry of hydrothermal vent fluids from the Main Endeavour Field, northern Juan de Fuca Ridge: Geochemical controls in the aftermath of June 1999 seismic events, *J. Geophys. Res.*, *108*(B9), 1–23, doi:10.1029/2004JB003219.

Singh, S., R. P. Lowell, and K. C. Lewis (2013), Numerical modeling of phase separation at Main Endeavour Field, Juan de Fuca Ridge, *Geochem. Geophys. Geosyst.*, *14*, 4021–4034, doi:10.1002/ggge.20249.

Tivey, M. A, and H. P. Johnson (2002), Crustal magnetisation reveals subsurface structure of Juan de Fuca Ridge Hydrothermal System, *Geology*, *30*(11), 979–982, doi:10.1130/0091-7613(2002)030.

Van Ark, E. M., R. S. Detrick, J. P. Canales, S. M. Carbotte, A. J. Harding, G. M. Kent, M. R. Nedimovic, W. S. D. Wilcock, J. B. Diebold, and J. M. Babcock (2007), Seismic structure of the Endeavour Segment, Juan de Fuca Ridge: Correlations with seismicity and hydrothermal activity, *J. Geophys. Res.*, *112*, B02401, doi:10.1029/2005JB004210.

Von Damm, K. L., M. D. Lilley, W. C. Shanks, M. Brockington, A. M. Bray, K. M. O'Grady, E. Olson, A. Graham, G. Proskurowski, and S. S. Party (2003), Extraordinary phase separation and segregation in vent fluids from the southern East Pacific Rise, *Earth Planet. Sci. Lett.*, *206*(3–4), 365–378, doi:10.1016/S0012-821X(02)01081-6.

Weekly, R. T., W. S. D. Wilcock, D. R. Toomey, E. E. E. Hooft, and E. Kim (2014), Upper crustal seismic structure of the Endeavour segment, Juan de Fuca Ridge from traveltime tomography: Implications for oceanic crustal accretion, *Geochem. Geophys. Geosyst.*, *15*, 1296–1315, doi:10.1002/2013GC005159.

Weis, P., T. Driesner, D. Coumou, and S. Geiger (2014), Hydrothermal, multiphase convection of H_2O-NaCl fluids from ambient to magmatic temperatures: A new numerical scheme and benchmarks for code comparison, *Geofluids*, *14*(3), 347–371, doi:10.1111/gfl.12080.

Wells, J. T., and M. S. Ghiorso (1991), Coupled fluid flow and reaction in mid-ocean ridge hydrothermal systems: The behaviour of silica, *Geochim. Cosmochim. Acta*, *55*, 2467–2481.

Wilcock, S. D. (1998), Circulation and the temperatures of black smoker fluids Seafloor, *J. Geophys. Res.*, *103*, 2585–2596.

Wilcock, W. S. D. (2004), Physical response of mid-ocean ridge hydrothermal systems to local earthquakes, *Geochem. Geophys. Geosyst.*, *5*, Q11009, doi:10.1029/2004GC000701.

Wilcock, W. S. D., E. E. E. Hooft, D. R. Toomey, P. R. McGill, A. H. Barclay, D. S. Stakes, and T. M. Ramirez (2009), The role of magma injection in localizing black-smoker activity, *Nat. Geosci.*, *2*(7), 509–513, doi:10.1038/ngeo550.

Xu, G., D. R. Jackson, K. G. Bemis, and P. A. Rona (2014), Time-series measurement of hydrothermal heat flux at the Grotto mound, Endeavour Segment, Juan de Fuca Ridge, *Earth Planet. Sci. Lett.*, *404*, 220–231, doi:10.1016/j.epsl.2014.07.040.